Journal of Alloys and Compounds 623 (2015) 367–373

Contents lists available at ScienceDirect

Journal of Alloys and Compounds

journal homepage: www.elsevier.com/locate/jalcom

Effects of Na content on structural and optical properties of Na-doped ZnO thin films prepared by sol–gel method

L.W. Wang [a], F. Wu [a,*], D.X. Tian [a,b], W.J. Li [a], L. Fang [a,*], C.Y. Kong [b,*], M. Zhou [a]

[a] State Key Laboratory of Power Transmission Equipment & System Security and New Technology, College of Physics, Chongqing University, Chongqing 400044, PR China
[b] Key Laboratory of Optoelectronic Functional Materials, Chongqing Normal University, Chongqing 401331, PR China

ARTICLE INFO

Article history:
Received 13 July 2014
Received in revised form 25 October 2014
Accepted 8 November 2014
Available online 15 November 2014

Keywords:
Na-doped ZnO thin films
Sol–gel method
Structural properties
Photoluminescence

ABSTRACT

In this paper, Na-doped ZnO (NZO) thin films with doping contents of 3–30 at.% were synthesized on quartz glass substrates by sol–gel spin coating method. The structure, morphology, optical transmittance and photoluminescence properties of NZO films were characterized by X-ray diffraction (XRD), field emission scanning electron microscope (FESEM), atomic force microscope (AFM), UV–VIS spectrometer and fluorescence spectrophotometer, respectively. The results showed that all the NZO thin films exhibit a strong preferential *c*-axis orientation with a hexagonal polycrystalline structure. An apparent increase in crystallinity was observed with the increasing Na content. The surface of the heavily Na doped samples (30 at.%) exhibits nanorods morphology. The RMS roughness changed from 16.219 nm to 53.072 nm with the increase of Na concentrations. As Na doping content increases to 24 at.%, the average transmittance was still larger than 62% in the visible range. The optical band gap initially increased and then decreased nearly linearly with the increase of Na content. The refractive index of NZO films in the visible range was found to increase gradually with increasing Na dopants. Room temperature photoluminescence (PL) spectra showed sharp ultraviolet emissions centered at 388 nm and broad green–yellow emissions (450–650 nm). The violet emission centered at 424 nm appeared in the spectra of 30 at.% NZO. In addition, it was found that the low Na doping concentration contributed to the enhancement of I_{NBE}/I_{DLE}.

1. Introduction

Recently, ZnO exhibiting a wide optical band gap of 3.37 eV and a large exciton binding energy of 60 meV at room temperature has received great attention owing to its promising applications in optoelectronic devices such as light emitting diodes, laser diodes and photodetectors [1]. Optical constants are the fundamental properties for optical materials, which is considerably important for device design. The optical constants of undoped [2], Li doped [3] and In doped [4] ZnO thin films were investigated in previous reports. It is possible to evaluate optical constants, such as absorption coefficient, refractive index and dielectric constant by analyzing transmittance spectrum [5–7]. Furthermore, it is necessary to clearly understand the luminescence behavior of ZnO for designing optoelectronic devices and improving its UV emitting performance. This is due to the fact that a large amount of defects such as Zinc interstitials and oxygen vacancies contribute to the visible emissions and even deteriorate the near band-edge emission.

Potential applications in optoelectronics device necessitate better understanding of the factors controlling the structural and optical properties of ZnO films. Owing to the different structure of the electronic shell and the similar size of Na and Zn, the group I element Na for Zn sites has been considered as a good candidate to modify the structural, optical, physical, and chemical properties of ZnO [8–10]. In addition, first-principle calculations reveal that Na can enter the ZnO lattice interstitially in combination with a neighboring oxygen vacancy [11,12]. However, there are a relatively few papers on the reports of NZO prepared by a variety of techniques. Lu et al. [13] grew NZO thin films on different substrates at 400 °C using a low-pressure MOCVD method. Lin et al. [14] deposited NZO with the codoping of H and Na by pulsed laser deposition (PLD). Liu et al. [1] reported the first demonstration of the synthesis of single-crystalline Na-doped p-type ZnO microwires using chemical vapor deposition (CVD). Ilican prepared NZO nanorods by sol–gel method and characterized by XRD, SEM, XPS and spectrophotometer [15]. Wang and Gao [16] deposited NZO thin films on Si (100) substrates with sol–gel method and discussed the influence of annealing temperature on structural and optical properties. With the advantages of homogeneous dispersion of dopants in ZnO lattice based on hydrolysis and condensation

* Corresponding authors. Tel.: +86 23 65678369.
E-mail addresses: fang01234@163.com (F. Wu), lfang@cqu.edu.cn (L. Fang), kchy@163.com (C.Y. Kong).

http://dx.doi.org/10.1016/j.jallcom.2014.11.055
0925-8388/

reactions, low cost, easy fabrication of large-area and so on, sol–gel is one of the most promising deposition techniques. In this paper, NZO films were fabricated on quartz glass substrates by sol–gel spin coating method. The influences of Na content (3–30 at.%) on the film structural and optical properties were investigated systematically.

2. Experimental details

2.1. Thin film preparation

NZO thin films with different doping contents were prepared on quartz glass substrates by sol–gel spin coating method. Zinc acetate dihydrate ($Zn(CH_3COO)_2 \cdot 2H_2O$), 2-methoxyethanol ($CH_3O(CH_2)_2OH$), monoethanolamine (MEA) and NaCl were used as the starting precursors, solvent, sol stabilizer, and Na dopant source respectively. All of the materials were purchased from Aladdin chemicals. The concentration of the zinc acetate was 0.75 M, and the molar ratio of MEA to zinc acetate was maintained at 1.0. The [Na/(Na + Zn)] atom ratios in the solution were 0, 3, 6, 12, 24, 30 at.%, respectively. The mixed solution was stirred at 70 °C for 2 h to yield a clear and homogeneous solution, serving as the spin coating solution after aging for 48 h at room temperature. Prior to the deposition, the quartz glass substrates were ultrasonically cleaned in acetone, alcohol and deionized water for 10 min respectively, and subsequently dried in a nitrogen stream. The resultant sol was dropped onto the clean substrates, which were rotated at 3000 rpm for 20 s. After each coating step, the films dried at 300 °C for 10 min to evaporate the solvent and remove organic residuals. The spin coating procedure was repeated ten times to obtain desired film thickness. Finally, all the samples were annealed in the tube furnace at 800 °C for 1 h under ambient atmosphere.

2.2. Characterization methods

The crystal structure of NZO films were investigated by X-ray diffraction (XRD PW1710) using the Cu Kα line (λ = 1.5406 Å) and the scanning range of 2θ was between 30° and 75°. During the measurements, the excitation voltage, the tube current and the scanning speed were maintained at 40 kV, 40 mA, and 4°/min, respectively. The surface morphologies of the as-prepared samples were examined with field emission scanning electron microscope (FE-SEM, Nova400) and atomic force microscope (AFM, CSPM-4000). The optical transmittance of the samples were investigated by using UV–VIS spectrophotometer (UV-3600) in the range of 300–800 nm. The room temperature PL spectra was measured by a spectraphotometer (RF-5301) with an excitation wavelength of 325 nm.

The thicknesses of all the films were investigated to be about 300 nm as measured by a step instrument (AMBIOS). An inductively coupled plasma optima optical emission spectrometer (ICP–OES) was used to identify the Na incorporation into ZnO. According to the ICP–OES measurement, the atomic ratio of Na in the doped films were 0%, 2.9%, 6.1%, 11.7%, 23.8% and 29.6%, respectively. Those were nearly equal to stoichiometry in resultant sol.

3. Results and discussion

3.1. Structural properties

Fig. 1 shows the XRD patterns of pure ZnO and NZO thin films with various Na contents. It can be seen that both the pure and NZO films exhibit polycrystalline hexagonal wurtzite structures with all XRD peaks. No phases related to Na or Na compound are observed at different doping level within the XRD detection limits, indicating that Na^+ might substitute Zn^{2+} or incorporate into interstitial sites in the ZnO lattice. For undoped ZnO films, the intensity of the (101) peak is higher than that of (002). But all the NZO films exhibit enhanced intensities corresponding to (002) peak when compared to (100) and (101) peaks, which indicates the preferential orientation along the *c*-axis. An apparent increase in crystallinity is also observed as suggested by the increase of the (002) peak intensity with the increasing Na content. In addition, the inset shows that the (002) peak positions shift toward lower angle as Na content increases from 0 to 24 at.%, further indicating dopants had been incorporated into ZnO films. It is reasonable that the substitution of Zn^{2+} with Na^+ leads to an expansion of the lattice constant due to the ionic radius difference between Zn^{2+} (0.74 Å) and Na^+ (0.95 Å). Furthermore, Liu et al. reported that with an increase of oxygen pressure, the (002) peak position of Na δ-doped ZnO thin films shifts to the lower diffraction angle side [17]. However, with further increase of Na content from 24 at.% to 30 at.%, a dramatical change that the (002) peak position shifts to a relatively higher angle is detected. Lü et al. [18] pointed out that Na interstitials are greater than Na substitutions in the heavily Na-doped ZnO film, which can explain the change.

Table 1 summarizes 2θ, FWHM of (002) peaks, lattice constants *c*, calculated average crystal size *D* and residual stress σ for the $Na_xZn_{1-x}O$ films samples. The instrumental contribution to the peak broadening was eliminated.

Average crystal sizes were calculated from the (002) peak using Scherrer formula [19]:

$$D = \frac{0.9\lambda}{\beta \cos\theta} \quad (1)$$

where *D*, λ, θ and β are the average crystal size, the X-ray wavelength (λ = 1.5406 Å), Bragg diffraction angle, and FWHM, respectively. The calculated results are listed in Table 1. As Na dopant increases from 3 at.% to 24 at.%, the average crystal size increases from 42.97 to 56.17 nm, indicating that a high Na content can improve the crystallinity of ZnO film. However, it is important to point out that there are no average crystallite size discussion and analysis for 30 at.% doped films due to the appearance of nanorod-like film shown in Fig. 2(f). Wang et al. [20] have reported that the Zn_i diffusion can promote the growth of ZnO crystal. The Na_{Zn} defects may increase the Zn_i defects. Therefore, the crystal size of $Na_xZn_{1-x}O$ films increases with the increasing of Na content.

The lattice constant c can be calculated by using the following formula [19]:

$$\frac{1}{d_{hkl}^2} = \frac{4}{3}\left[\frac{h^2 + hk + k^2}{a^2}\right] + \frac{l^2}{c^2} \quad (2)$$

where *a* and *c* are the lattice constants and d_{hkl} is the crystalline plane distance for indices (*hkl*). According to Eq. (2), *c* is equal to $2d_{hkl}$ for the (002) peak. The result shows that the lattice constants c of the NZO (3–24 at.%) are larger than that of the undoped one, implying that most of the Na^+ are accommodated at the substitutional sites. For the $Na_{0.30}Zn_{0.70}O$ sample, *c* become smaller even than that of the undoped one, which indicates that the Na ions are mostly incorporated as the Na_i donors.

For hexagonal crystals with a highly *c*-axis preferred orientation, the in-plane stress of the films can be calculated using the biaxial strain model [21],

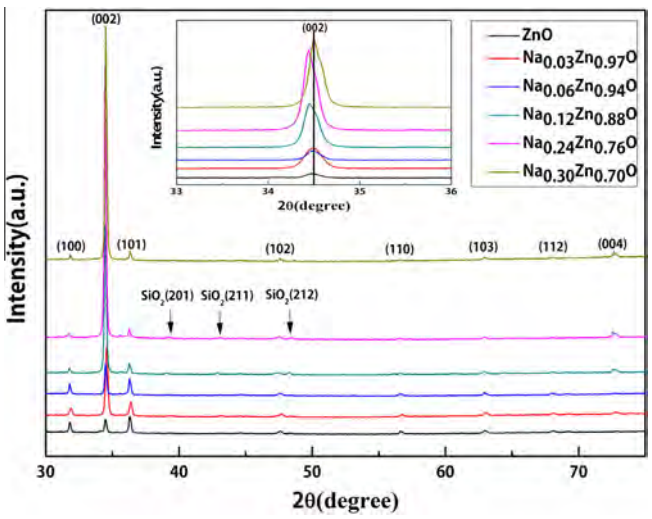

Fig. 1. XRD patterns of pure ZnO and NZO thin films with various Na contents.

Table 1
Structural parameters of pure ZnO and NZO films.

Samples	2θ (°)	FWHM (β)	D (nm)	c (Å)	σ (GPa)
ZnO	34.492	0.192	44.77	5.1964	0.744
$Na_{0.03}Zn_{0.97}O$	34.432	0.200	42.97	5.2052	−0.015
$Na_{0.06}Zn_{0.94}O$	34.433	0.166	51.77	5.2050	−0.002
$Na_{0.12}Zn_{0.88}O$	34.415	0.167	51.46	5.2077	−0.230
$Na_{0.24}Zn_{0.76}O$	34.403	0.153	56.17	5.2094	−0.383
$Na_{0.30}Zn_{0.70}O$	34.503	0.148	–	5.1948	0.883

$$\sigma = 4.5 \times 10^{11} \frac{c_0 - c}{c_0} \quad (3)$$

where c_0 is the corresponding value for bulk ZnO (5.205 Å) and c is the lattice parameter of films obtained from XRD result. The positive (negative) sign of σ indicates that the films are in a state of tensile (compressive) press. As seen in Table 1, the stress is compressive with the Na content in a range of 3–24 at.%, and the absolute value increases with the increasing of dopant. While the compressive stress transformed to tensile stress with the Na doping constant increasing from 24 at.% to 30 at.%. The dramatic change may be due to lots of Na interstitials in the heavily Na-doped ZnO film.

3.2. Surface morphologies

Fig. 2 presents the FESEM images of pure and NZO films. The pure ZnO shows a wrinkle network with spherical nanoparticles, which can also be seen from the AFM image in the inset of Fig. 3(a). As shown in Fig. 2(b)–(f), the wrinkle structure almost disappears and the increase in the grain size can be observed with the increasing of Na content. As Na doping content increases from 3 to 6 at.%, the samples show denser morphology without visible

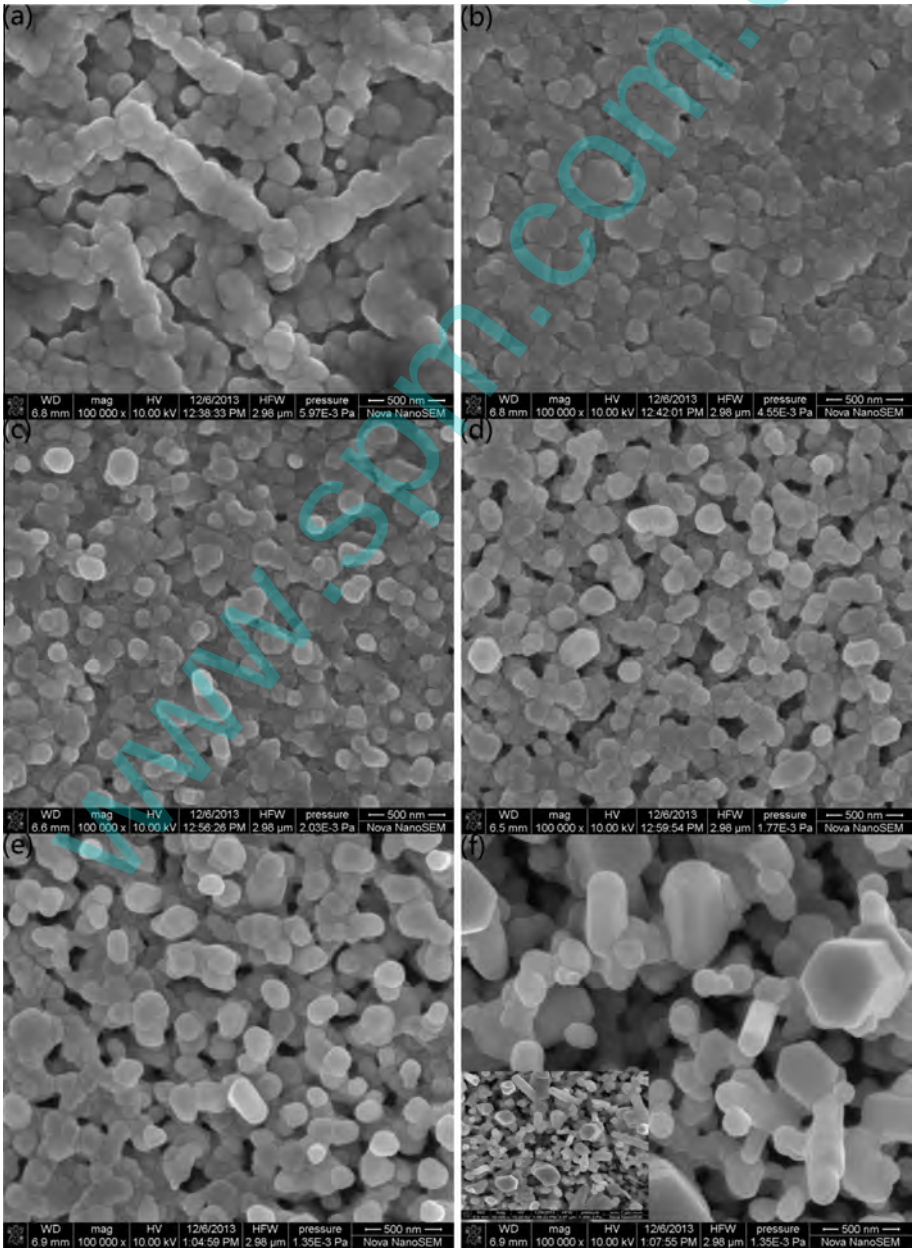

Fig. 2. FESEM images of pure ZnO and NZO films: (a) ZnO, (b) $Na_{0.03}Zn_{0.97}O$, (c) $Na_{0.06}Zn_{0.94}O$, (d) $Na_{0.12}Zn_{0.88}O$, (e) $Na_{0.24}Zn_{0.76}O$, (f) $Na_{0.30}Zn_{0.70}O$; the inset of (f) shows the FESEM image of $Na_{0.30}Zn_{0.70}O$ film with a magnification of 50,000.

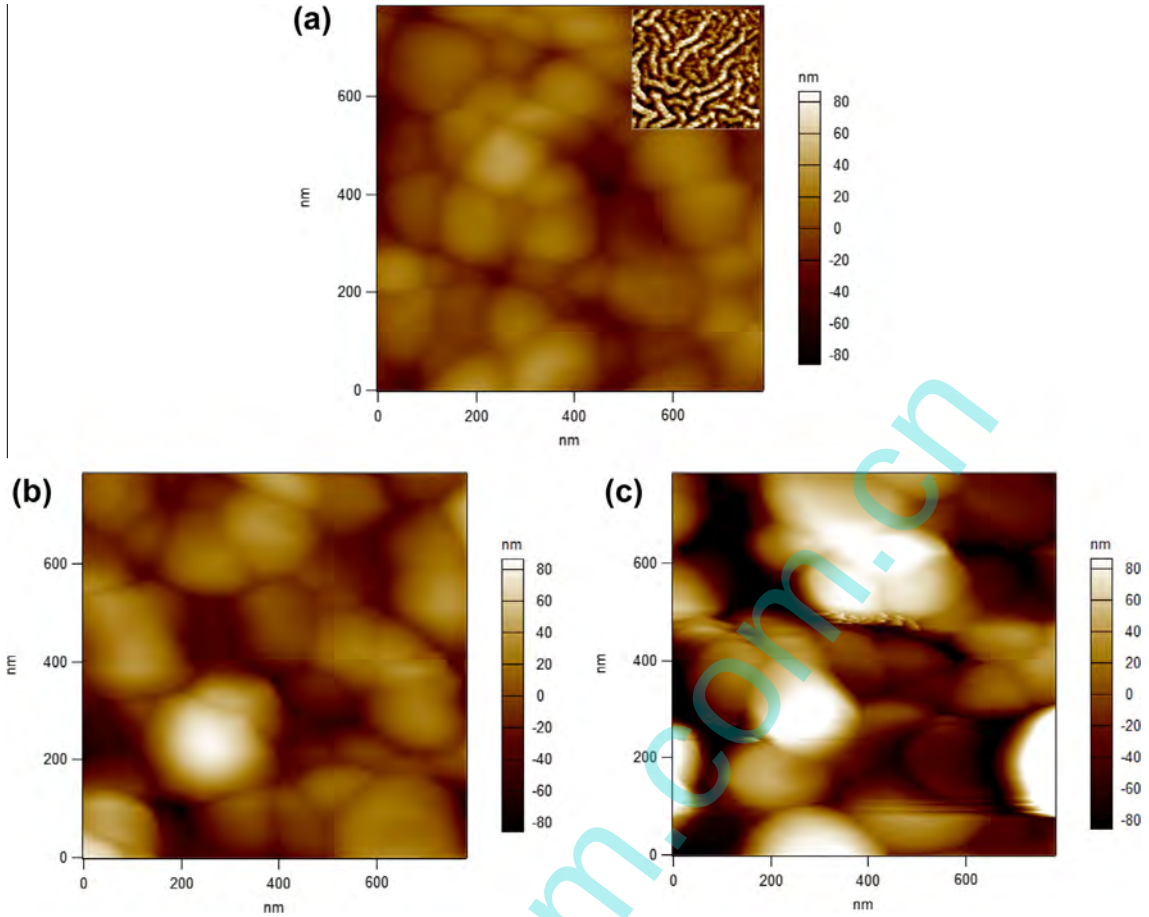

Fig. 3. AFM images of pure ZnO and NZO films: (a) 0 at.%; (b) 12 at.%; (c) 24 at.%; the inset shows the AFM scanning of pure ZnO film with a 10 μm × 10 μm range.

voids and defects overall the surface. However, many obvious voids were found when Na content further increases. Especially, the surface of the film doped 30 at.% Na exhibits nanorod shape. The *c*-axis orientation may be explained with the change of internal stress and surface free energy caused by Na doping content [22].

Fig. 3 shows the surface topographys of pure and NZO films. It can be observed that hexagonally faceted columnar grains play an important role in the surface morphology. The root mean square (RMS) roughness of the different films is obtained by the AFM scanning (800 nm × 800 nm). The surface roughness of films in Fig. 3(a)–(c) is 16.219, 25.791, 53.072 nm, respectively. As revealed by AFM images, both the surface roughness and the average grain size increase with an increase in doping ratio. The voids are existed on the loose surface of thin films when the doping content is 12–24 at.%. Furthermore, the grains coalesce and grow in the direction perpendicular to the substrate surface with Na incorporation. These results suggest that the increase of surface roughness along with the Na doping content may be attributed to the larger grain formation and increasing porosity of the films [23]. Geng et al. [24] have reported that the increasing roughness of Hf-doped ZnO films is induced by the preferred c-axis growth mode at high concentration Hf doping. However, Huang et al. [25] suggested that the RMS roughness of Mg doped ZnO films increased with the doping, which was due to the aggregation of MgO particles on the film surface.

3.3. Optical properties

Fig. 4 shows the transmittance spectra of pure ZnO and NZO films. It is clear that the pure ZnO films have an average transmittance higher than 71% in the visible range, and the transmittance decreases with the increase of Na content. Lv et al. [26] have reported that the transmittance in the visible light wavelength range decreases with the increase of Na content, and is only about 40% when the Na/Zn ratio is 6 at.%. However, for the obtained samples, as Na doping content increases to 24 at.%, the average transmittance is still larger than 62% in the visible range, which is profitable for the application in optical devices. Compared with the pure ZnO film, the UV absorption edge of NZO films shows a red-shift after Na incorporation.

The absorption coefficient α is calculated by Eq. (4) [27–29]

$$\alpha = -\ln T/d \tag{4}$$

where T is the transmittance, d is the film thickness.

For the direct transition semiconductor, the optical band gap E_g can be obtained by using the following equations [27–29]:

$$\alpha h\nu = A(h\nu - E_g)^{1/2} \tag{5}$$

where α is the absorption coefficient, A is the constant for a direct transition, h is the Planck's constant, and ν is the photon frequency. The value of E_g is given by the linear extrapolation of the plot of $(\alpha h\nu)^2$ versus $h\nu$ to the energy axis. The optical band gap as a function of Na content is shown in the inset of Fig. 4. It shows that the optical band gap of NZO films initially increases nearly linearly as the doping content increases to 6 at.% and then decreases nearly linearly with an increase of Na content. Xu et al. [30] reported that the optical band gap of the K-doped ZnO thin films by the sol–gel method increased at first and then decreased with the increasing K content. In the present study, the optical band gap E_g of $Na_xZn_{1-x}O$ film can be expressed in terms of Na doping content (x):

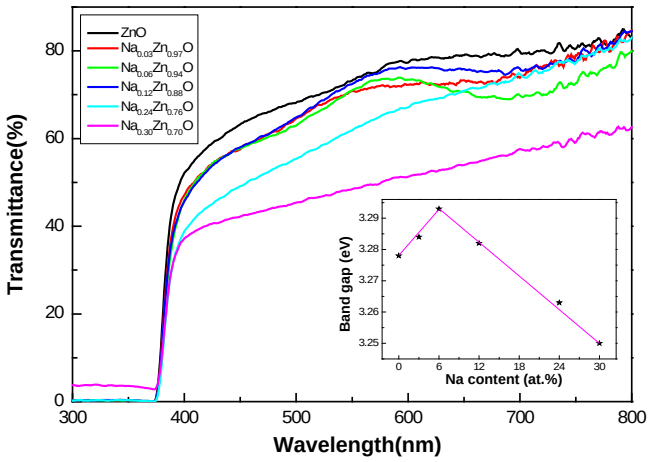

Fig. 4. Optical transmittance spectra of pure ZnO and NZO films. Inset shows the optical band gap as a function of Na content.

$$E_g = 0.0025x + 3.278,\ 0 \le x \le 6\ \text{at.}\% \quad (6)$$

$$E_g = -0.0018x + 3.282,\ 6\ \text{at.}\% \le x \le 30\ \text{at.}\% \quad (7)$$

Noteworthily, the band gap increases from 3.278 eV (for the pure ZnO) to 3.293 eV (for the 6 at.% NZO). The band gap extension of the lightly Na doped ZnO film can be attributed to the decrease of n-type carrier concentration, which is explained by a combined effect of the increased substitutional Na (Na_{Zn}) density and the decreased oxygen-vacancy (V_O) density [31,32]. For the heavily Na doped ZnO, a great majority of Na_i defects may induce impurity levels near the valence band maximum (VBM) and conduction band minimum (CBM), resulting in the decrease of band gap from 3.293 to 3.25 eV. Previously, Bahşi and Oral [33] revealed that the band tails resulted from doping could lead to a large number of band-to-tail and tail-to-tail transitions and thus the absorption edge shifts to longer wavelength.

Refractive index is one of the fundamental properties for an optical material, because it is closely related to the electronic polarizability of ions and the local field inside materials. The evaluation of refractive indices of optical materials is considerably important for the applications in integrated optic devices [26]. The refractive index of Na:ZnO films can be determined from the following equation [34]:

$$n = \left[\frac{1+R}{1-R}\right] + \sqrt{\frac{4R}{(1-R)^2} - k^2} \quad (8)$$

$$k = \frac{\alpha\lambda}{4\pi} \quad (9)$$

where R is the reflectance, and k is the extinction coefficient. Using the transmittance, absorption coefficient and film thickness, R values were calculated. Fig. 5(a) and (b) show the refractive index and extinction coefficients of NZO films with different Na content in the range of 370–700 nm. Both the refractive index and extinction coefficient of all samples decrease along with the wavelength. It can also be seen that the n values and k values increase with the increasing doping content. In general, the refractive index of single crystal ZnO is about 2.0. However, it was found that the average refractive index of all the obtained films in the visible range was about 2.4–3.6 in our study.

The fundamental electron excitation spectrum of the film was described by means of a frequency dependent of the complex electronic dielectric constant. Real and imaginary parts of the dielectric constant are related to the n and k values. The real and imaginary parts can be calculated by using the following formulas [35]:

$$\varepsilon_1 = n^2(\lambda) - k^2(\lambda) \quad (10)$$

$$\varepsilon_2 = 2n(\lambda)k(\lambda) \quad (11)$$

The real ε_1 and imaginary ε_2 parts as a function of wavelength are shown in Fig. 5(c) and (d), respectively. It can be seen that the ε_1 values and ε_2 values increase slightly with the increasing Na dopant. It is obvious that the ε_1 values are higher than that of ε_2.

3.4. Photoluminescence properties

Fig. 6 shows the room temperature PL spectra of pure and NZO films. The PL results are found to be strongly dependent on the Na content. Generally, the intrinsic ZnO usually exhibits an intense ultraviolet (UV) emission peak which originates from the radiative recombination of free excitions corresponding to the near-band edge emission (NBE) of ZnO and a broad visible emission [36]. Two main peaks appeared in the PL spectra, the sharp ultraviolet emission centered at 388 nm (3.19 eV) and the broad green–yellow emission (450–650 nm). Fig. 6 shows that with increases of Na content, intensity of the ultraviolet emission increases initially when the doping content is 3 at%, and then decreases with higher Na doping concentration. Similarly, Xu et al. [30] have also found that the ultraviolet emission become intense after 1 at.% K is doped in ZnO thin film, while it reduces suddenly when the K doping content increases. However, a dramatical phenomenon appeared in the visible emission. The intensity of the visible emission decreases firstly, then increases slightly and decreases rapidly at last. It's worth mentioning that the violet emission centered at 424 nm (2.92 eV) in the range of 380–450 nm appears as the doping content reaches 30 at.%, which has been also reported in earlier researches. Peng et al. [37] have found the violet emission band at 410 nm appeared in the Cu-doped ZnO films, and they consider that the violet emission is associated with zinc vacancy. Jin et al. [38] have reported that the violet emission centered at 420 nm appeared in the ZnO films by pulsed laser deposition, which might be attributed to defects of the grain boundaries. According to energy level diagram of defects in ZnO [39], the energy interval between the zinc interstitial defect level and the valence band is about 2.9 eV, which is consistent with the energy of violet emission at 424 nm (2.92 eV). Therefore, the violet emission can be ascribed to the zinc interstitial defect level and defects level in the grain boundaries.

When the doping content is greater than 3 at%, a strong deep level emission (DLE) centered at around 530 nm is dominated in the PL spectrum, which is the most commonly observed defect emission in ZnO nanostructures. This deep level emission can be commonly attributed to the oxygen vacancies [40–42]. It is found that the low doping concentration contributes to enhancement of the UV emission and reduction of the deep level emission, which is consistent with previous work reported by Yang et al. [43]. The ratio for the intensity of NBE emission (I_{NBE}) to that of DLE emission (I_{DLE}) increases from 2.27 (for ZnO) to 4.74 (for 3 at% Na doped ZnO). This result may be explained by the suppressing of V_O defects by the Na doping and the passivation of present V_O defects by the formation of $(Na_{Zn}–V_O)^{+/0}$ complexes. Unfortunately, the ratio of I_{NBE}/I_{DLE} declines obviously when the doping content is over 3 at%, indicating the intensity of near band edge emission is suppressed. These results also prove that Na interstitials are more than Na substitutions in the NZO thin film for higher doping content, which leads to the reduction in the formation of $(Na_{Zn}–V_O)^{+/0}$ complexes.

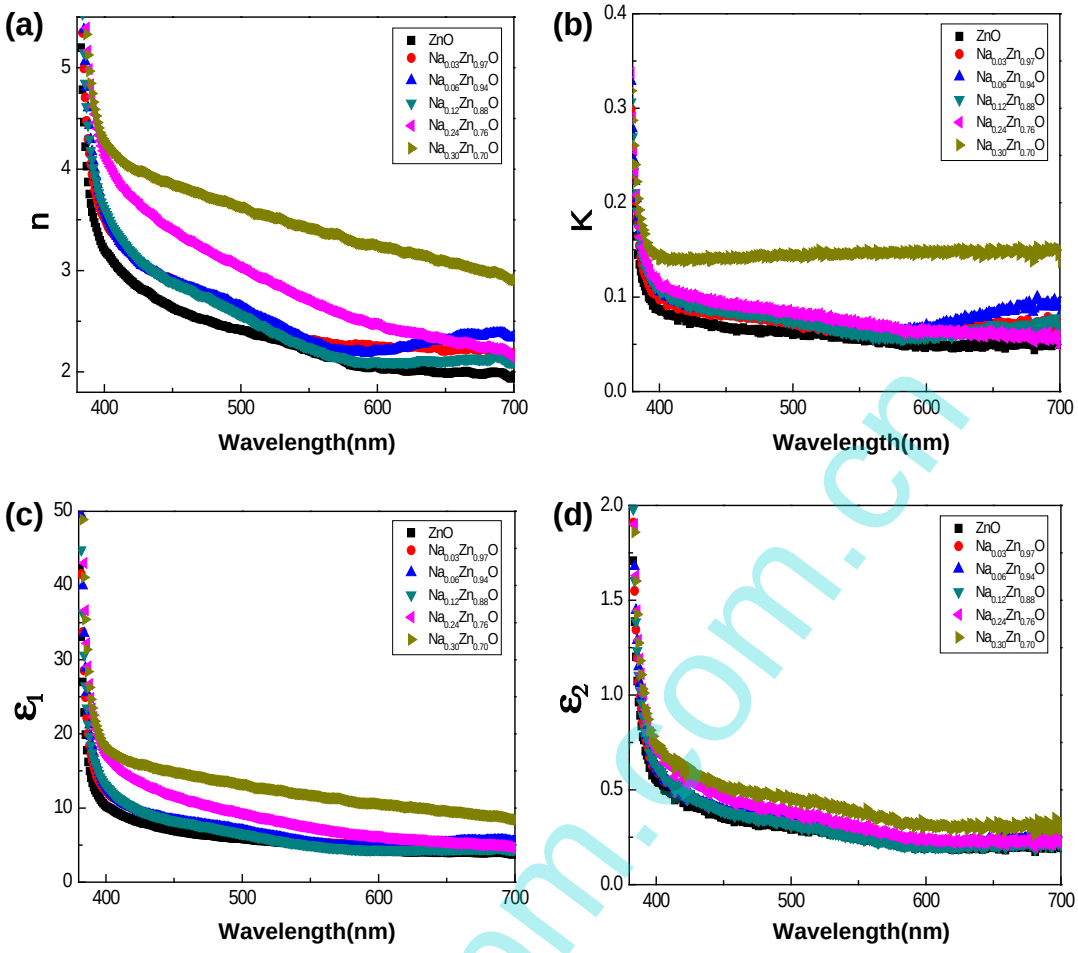

Fig. 5. Effect of Na content on the refractive index (a), extinction coefficient (b), real (c) and imaginary (d) parts of dielectric constants for NZO films.

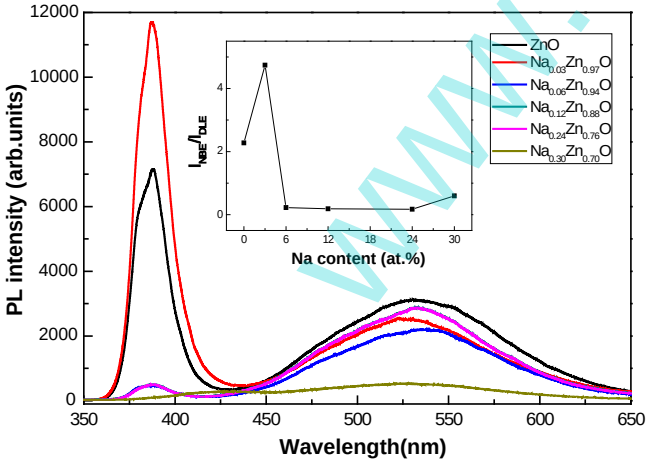

Fig. 6. Room temperature PL spectra of pure ZnO and NZO films. Inset shows I_{NBE}/I_{DLE} as a function of Na content.

4. Conclusions

In summary, NZO films were synthesized via the sol–gel method on quartz substrates. The effects of Na content on the structural and optical properties of NZO films were investigated systematically. The results show that the obtained NZO films are highly c-axis orientated. An apparent increase in crystallinity is observed with increasing Na content. The surface of the heavily Na doped samples (30 at.%) exhibits nanorods morphology. The increase of surface roughness along with the Na content may be attributed to the larger grain formation and more porosity of the films. As Na doping content increases from 3 at.% to 24 at.%, the average transmittance for the obtained samples is still larger than 62% in the visible range. The optical band gap initially increases and then decreases nearly linearly with an increase of Na content owing to a combine effect of the ratio of Na_{Zn} to Na_i defects and V_O defects. The refractive index of NZO thin films can be controlled by the Na doping content, which contributes to the applications in designing integrated optic devices. PL spectra shows two main peaks: a sharp ultraviolet emission centered at 388 nm and a broad green–yellow emission (450–650 nm). The violet emission centered at 424 nm appeared in the spectra of 30 at.% NZO. It was found that the low doping concentration contributes to the enhancement of I_{NBE}/I_{DLE} ratio, which can be explained by the suppressing of V_O defects by the Na doping and the passivation of present V_O defects by the formation of $(Na_{Zn}–V_O)^{+/0}$ complexes.

Acknowledgments

This work was financially supported by the National Natural Science Foundation of China (Grant Nos. 11074314, 11304405 and

51472038) and the Nature Science Foundation of Chongqing (Grant Nos. CSTC2013jjB0023, CSTC2012gg-gjhz50001, CSTC2013jcyj A50031), D&R Projects of Chongqing Education Commission under Grant No. KJ132209, the Fundamental Research Funds for the Central Universities (CDJZR12138801, CDJZR14135502 and CQDXW L2012017), the Visiting Scholarship of State Key Laboratory of Power Transmission Equipment & System Security and New Technology (2007DA10512711403) and the Sharing Fund of Large-scale Equipment of Chongqing University (Grant Nos. 2013121560 and 2013121561).

References

[1] W. Liu, F.X. Xiu, K. Sun, Y.H. Xie, K.L. Wang, Y. Wang, J. Zou, Z. Yang, J.L. Liu, Na-doped p-type ZnO microwires, J. Am. Chem. Soc. 132 (2010) 2498–2499.
[2] S.W. Xue, X.T. Zu, W.L. Zhou, H.X. Deng, X. Xiang, L. Zhang, H. Deng, Effects of post-thermal annealing on the optical constants of ZnO thin film, J. Alloys Comp. 448 (2008) 21–26.
[3] A. Abu EL-Fadl, Galal A. Mohamad, A.B. Abd El-Moiz, M. Rashad, Optical constants of $Z_{n1-x}Li_xO$ films prepared by chemical bath deposition technique, Physica B 366 (2005) 44–54.
[4] M. Caglar, S. Ilican, Y. Caglar, Influence of dopant concentration on the optical properties of ZnO: in films by sol–gel method, Thin Solid Films 517 (2009) 5023–5028.
[5] T. Güngör, B. Saka, Calculation of the optical constants of a thin layer upon a transparent substrate from the reflection spectrum using a genetic algorithm, Thin Solid Films 467 (2004) 319–325.
[6] S.W. Xue, X.T. Zu, W.G. Zheng, H.X. Deng, X. Xiang, Effects of Al doping concentration on optical parameters of ZnO: Al thin films by sol–gel technique, Physica B 381 (2006) 209–213.
[7] D.A. Minkov, Calculation of the optical constants of a thin layer upon a transparent substrate from the reflection spectrum, J. Phys. D. Appl. Phys. 22 (1989) 1157–1161.
[8] C.H. Park, S.B. Zhang, S.H. Wei, Origin of p-type doping difficulty in ZnO: the impurity perspective, Phys. Rev. B 66 (2002) 073202.
[9] S.B. Orlinskii, J. Schmidt, P.G. Baranov, D.M. Hofmann, C.D. Donegá, A. Meijerink, Probing the wave function of shallow Li and Na donors in ZnO nanoparticles, Phys. Rev. Lett. 92 (2004) 047603.
[10] S.S. Lin, J.G. Lu, Z.Z. Ye, H.P. He, X.Q. Gu, L.X. Chen, J.Y. Huang, B.H. Zhao, P-type behavior in Na-doped ZnO films and ZnO homojunction light-emitting diodes, Solid State Commun. 148 (2008) 25–28.
[11] E.C. Lee, K.J. Chang, Possible p-type doping with group-I elements in ZnO, Phys. Rev. B 70 (2004) 115210.
[12] Ü. Özgür, Y.I. Alivov, C. Liu, A. Teke, M.A. Reshchikov, S. Doğan, V. Avrutin, S.J. Cho, H. Morkoc, A comprehensive review of ZnO materials and devices, J. Appl. Phys. 98 (2005) 041301.
[13] Y.F. Lu, K.W. Wu, Y.J. Zeng, Z.Z. Ye, J.Y. Huang, L.P. Zhu, B.H. Zhao, Local p-type conduction of Na-doped ZnO thin films grown by MOCVD, Chem. Phys. Lett. 582 (2013) 82–85.
[14] S.S. Lin, H.P. He, Y.F. Lu, Z.Z. Ye, Mechanism of Na-doped p-type ZnO films: suppressing Na interstitials by codoping with H and Na of appropriate concentrations, J. Appl. Phys. 106 (2009) 093508.
[15] S. Ilican, Effect of Na doping on the microstructures and optical properties of ZnO nanorods, J. Alloys Comp. 553 (2013) 225–232.
[16] D.Y. Wang, S.X. Gao, Influence of annealing condition on the structure and optical properties of Na-doped ZnO thin films prepared by sol–gel method, J. Alloys Comp. 476 (2009) 925–928.
[17] H.B. Liu, X.H. Pan, J.Y. Huang, H.P. He, Z.Z. Ye, Preparation of Na delta-doped p-type ZnO thin films by pulsed laser deposition using NaF and ZnO ceramic targets, Thin Solid Films 540 (2013) 53–57.
[18] J.G. Lü, K. Huang, J.B. Zhu, X.M. Chen, X.P. Song, Z.Q. Sun, Preparation and characterization of Na-doped ZnO thin films by sol–gel method, Physica B 405 (2010) 3167–3171.
[19] B.D. Cullity, S.R. Stock, Elements of X-ray Diffraction, Addison-Wesley, Reading, MA, 1978.
[20] T. Wang, Y.M. Liu, Q.Q. Fang, M.Z. Wu, X. Sun, F. Lu, Low temperature synthesis wide optical band gap Al and (Al, Na) co-doped ZnO thin films, Appl. Surf. Sci. 257 (2011) 2341–2345.
[21] C.L. Tsai, M.S. Wang, Y.H. Chen, H.C. Chang, C.J. Liu, C.T. Lee, Y.T. Shih, H.J. Huang, Y.J. Lin, Effects of Li content on the structural, optical, and electrical properties of LiZnMgO films, J. Appl. Phys. 107 (2010) 113717.
[22] D.H. Bao, H.S. Gu, A.X. Kuang, Sol–gel-derived c-axis oriented ZnO thin films, Thin Solid Films 312 (1998) 37–39.
[23] N. Kakati, S.H. Jee, S.H. Kim, J.Y. Oh, Y.S. Yoon, Thickness dependency of sol–gel derived ZnO thin films on gas sensing behaviors, Thin Solid Films 519 (2010) 494–498.
[24] Y. Geng, Z.Y. Xie, W. Yang, S.S. Xu, Q.Q. Sun, S.J. Ding, H.L. Lu, D.W. Zhang, Structural, optical, and electrical properties of Hf-doped ZnO films deposited by atomic layer deposition, Surf. Coat. Technol. 232 (2013) 41–45.
[25] K. Huang, Z. Tang, L. Zhang, J.Y. Yu, J.G. Lv, X.S. Liu, F. Liu, Preparation and characterization of Mg-doped ZnO thin films by sol–gel method, Appl. Surf. Sci. 258 (2012) 3710–3713.
[26] J.G. Lv, K. Huang, X.M. Chen, J.B. Zhu, C.B. Cao, X.P. Song, Z.Q. Sun, Optical constants of Na-doped ZnO thin films by sol–gel method, Opt. Commun. 284 (2011) 2905–2908.
[27] S. Ilican, M. Caglar, Y. Caglar, Sn doping effects on the electro-optical properties of sol gel derived transparent ZnO films, Appl. Surf. Sci. 256 (2010) 7204–7210.
[28] A.A. Ogwu, E. Bouquerel, O. Ademosu, S. Moh, E. Crossan, F. Placido, The influence of rf power and oxygen flow rate during deposition on the optical transmittance of copper oxide thin films prepared by reactive magnetron sputtering, J. Phys. D. Appl. Phys. 38 (2005) 266–271.
[29] W.T. Yen, Y.C. Lin, P.C. Yao, J.H. Ke, Y.L. Chen, Effect of post-annealing on the optoelectronic properties of ZnO: Ga films prepared by pulsed direct current magnetron sputtering, Thin Solid Films 518 (2010) 3882–3885.
[30] L.H. Xu, X.Y. Li, J. Yuan, Effect of K-doping on structural and optical properties of ZnO thin films, Superlattice Microstruct. 44 (2008) 276–281.
[31] S.K. Kim, S.A. Kim, C.H. Lee, H.J. Lee, S.Y. Jeong, C.R. Cho, The structural and optical behaviors of K-doped ZnO/Al_2O_3 (0001) films, Appl. Phys. Lett. 85 (2004) 419–421.
[32] J.J. Lai, Y.J. Lin, Y.H. Chen, H.C. Chang, C.J. Liu, Y.Y. Zou, Y.T. Shih, M.C. Wang, Effects of Na content on the luminescence behavior, conduction type, and crystal structure of Na-doped ZnO films, J. Appl. Phys. 110 (2011) 013704.
[33] Z.B. Bahşi, A.Y. Oral, Effects of Mn and Cu doping on the microstructures and optical properties of sol–gel derived ZnO thin films, Opt. Mater. 29 (2007) 672–678.
[34] N.A. Subrahamanyam, A Textbook of Optics, Brj Laboratory, Delhi, 1977.
[35] K.H. Kim, K.C. Park, D.Y. Ma, Structural, electrical and optical properties of aluminum doped zinc oxide films prepared by radio frequency magnetron sputtering, J. Appl. Phys. 81 (1997) 7764–7772.
[36] J.C. Li, Q. Cao, X.Y. Hou, Effects of Ag-induced acceptor defects on the band gap tuning and conductivity of Li: ZnO films, J. Appl. Phys. 113 (2013) 203518.
[37] X.P. Peng, J.Z. Xu, H. Zang, B.Y. Wang, Z.G. Wang, Structural and PL properties of Cu-doped ZnO films, J. Lumin. 128 (2008) 297–300.
[38] B.J. Jin, S. Im, S.Y. Lee, Violet and UV luminescence emitted from ZnO thin films grown on sapphire by pulsed laser deposition, Thin Solid Films 366 (2000) 107–110.
[39] H.Q. Wang, G.Z. Wang, L.C. Jia, C.J. Tang, G.H. Li, Polychromatic visible photoluminescence in porous ZnO nanotubes, J. Phys. D. Appl. Phys. 40 (2007) 6549–6553.
[40] K. Vanheusden, C.H. Seager, W.L. Warren, D.R. Tallant, J.A. Voigt, Correlation between photoluminescence and oxygen vacancies in ZnO phosphors, Appl. Phys. Lett. 68 (1996) 403–405.
[41] K. Vanheusden, W.L. Warren, C.H. Seager, D.R. Tallant, J.A. Voigt, B.E. Gnade, Mechanisms behind green photoluminescence in ZnO phosphor powders, J. Appl. Phys. 79 (1996) 7983–7990.
[42] R.C. Wang, C.P. Liu, J.L. Huang, S.J. Chen, ZnO symmetric nanosheets integrated with nanowalls, Appl. Phys. Lett. 87 (2005) 053103.
[43] X.P. Yang, J.G. Lu, H.H. Zhang, B. Lu, J.Y. Huang, C.L. Ye, Z.Z. Ye, Unexpected positive role of oxygen vacancies in Na-doped ZnO, J. Appl. Phys. 112 (2012) 113510.